A Compact 90° Three-Branch Beam Splitter Based on Resonant Coupling

H. A. Jamid, M. Z. M. Khan, and M. Ameeruddin

Abstract—A compact 90° three-branch beam splitter is proposed. The device relies on the use of a high contrast material system. It utilizes a rectangular resonant cavity for its operation, which ensures excitation of a resonant cavity mode with even symmetry in both the vertical and the horizontal directions. Numerical simulations using the method of lines (MOL) show that it is possible to control the power splitting ratio among the output arms over a wide range of values. In all the cases examined, the device reflectivity and the fraction of radiated power are kept low.

Index Terms—Beam splitters, method of lines, optical waveguides, power splitters, waveguide junctions.

I. INTRODUCTION

BEAM splitters are indispensable elements of integrated optical circuits (IOCs). They are used in modulators and switches. They are also used to split the optical power among the different components of the IOC. Various types of beam splitters have been reported in the past years. This includes beam splitters with various numbers of output arms, such as the 1×2 [1]–[5], 1×3 [6]–[11], and 1×4 [12] beam splitters. The various types of previously reported 1×3 (three branches) beam splitters have a variable power splitting ratio and the ability to produce equal power distribution [6]–[10]. In the following, we present a brief review of some of the three-branch beam splitters that have been reported in literature. The three-branch beam splitter reported in [6] utilizes a pair of triangular microprisms on both sides of the waveguide junction to control the power splitting ratio. A substrate microprism in addition to beam expanders were employed in the beam splitter reported in [7]. By controlling the length of the microprism and the widths of the two waveguide expanders, variable power splitting in the output branches can be achieved in this device. In [8], phase front accelerator regions were introduced between the three output arms of the beam splitter for controlling the output power distribution. A spacing area is introduced in the central output branch in the case of the beam splitter reported in [9] for the purpose of controlling the power coupled to the central output arm. The beam splitter reported in [10] utilizes a V-shaped coupling gap to control the power splitting ratio and to reduce the radiation loss. The common feature of the above-mentioned beam splitters is the use of a low index
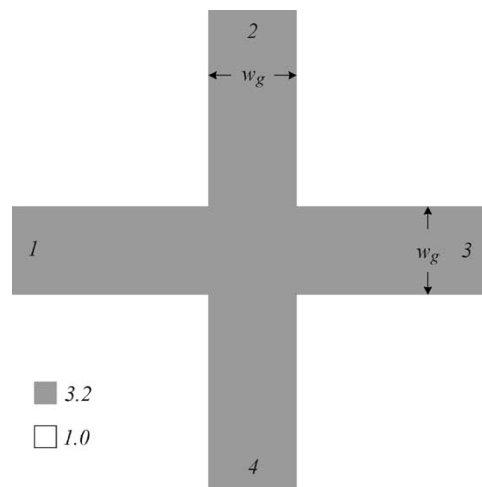
Fig. 1. Simple waveguide junction.

contrast material system, which imposes a maximum limit on the angle of the output arms with respect to the axis of the input arm. In addition, the use of a low index contrast material system results in relatively large device dimensions.

In this paper, we report a compact 90° three-branch beam splitter based on a high contrast material system for use in high-density integrated optics. An important distinguishing feature of the proposed device is that it utilizes a rectangular low-Q resonant cavity at the center to couple optical power efficiently into the output arms of the splitter. As we will see later, it is also possible to control the power splitting ratio of the device by adjusting the widths of the air gaps that separate the rectangular cavity from the four arms of the device.

II. PROPOSED STRUCTURE

Fig. 1 shows two identical slab waveguides that cross each other at a 90° angle forming a simple waveguide junction. The core width is $w_g = 0.2~\mu$m, and the core refractive index is 3.2. The cladding material is assumed to be air. These parameters have been chosen in order for the waveguides to be single mode at the wavelength range of interest. The TE$_0$ modal field is assumed to be incident on the junction from the input arm on the left-hand side of the structure. The modal reflectivity R_1 and the modal transmissivities in the upper, the forward, and the lower arms T_2, T_3, and T_4, respectively, have been calculated using the method of lines (MOL) [13]–[17]. Fig. 2(a)–(c) shows the spectral response of this simple waveguide junction including the fraction of the power radiated (FPR) and the total device loss (TDL $= R_1 +$ FPR). The results shown in Fig. 2
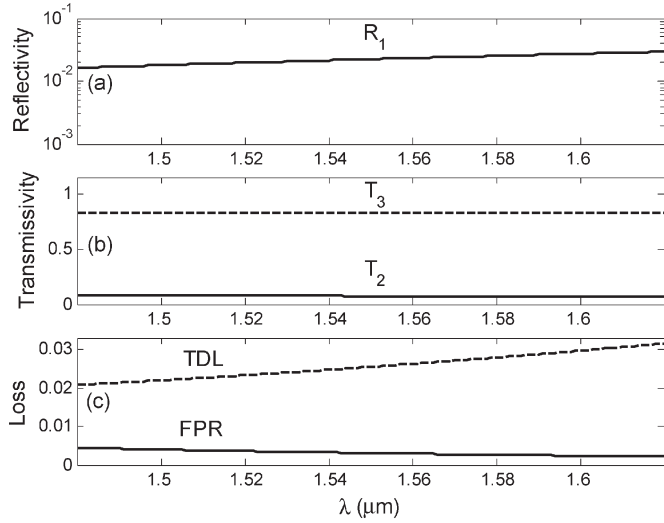
Fig. 2. Spectral response of the simple waveguide junction shown in Fig. 1.

Fig. 3. Proposed three-branch 90° beam splitter with a rectangular resonant cavity at the center.

have also been reported in [18]. The modal reflectivity response shown in Fig. 2(a) changes slowly with wavelength and reaches a value of about 3×10^{-2} at $\lambda = 1.62$ μm. Because of symmetry, the modal transmissivities in the vertical arms are equal to each other $(T_2 = T_4)$. The modal transmissivity in the vertical arms is nearly constant over the entire wavelength range of Fig. 2(b). It is generally small and is approximately 0.07 in value. The modal transmissivity in the forward arm T_3 is also shown in Fig. 2(b). The response in this case is also flat with an approximate modal transmissivity of about 0.83. The variation of the FPR with wavelength is shown in Fig. 2(c), which has a very small value of less than 5×10^{-3} in the entire wavelength range of the figure.

By inserting a square resonant cavity of an appropriate dimension at the center of the simple waveguide junction of Fig. 1, it is possible to form a waveguide crossing, with improved features as reported in [18] and [19]. By exciting the horizontally odd mode of the square cavity, the power coupled to the vertical arms (crosstalk) of the waveguide crossing is minimized. In this case, maximum power is coupled to the forward arm with a low modal reflectivity in the input arm.

Rather than inhibiting power coupling to the vertical arms as done in the above-mentioned waveguide crossing with a square cavity, we propose instead to enhance coupling to the vertical arms. By reducing the width of the square resonant cavity in the horizontal direction, thus, forming a rectangular cavity, the horizontally odd resonant cavity mode becomes cutoff, which ensures that the input field excites a resonant cavity mode with an even symmetry in the horizontal direction. This should, in turn, enhance coupling to the fundamental modes of the vertical arms. We will demonstrate through a number of numerical examples that this concept, under proper conditions, can lead to a large and controllable enhancement of the optical power coupled to the vertical arms of the structure. This can be done while maintaining small power reflection into the input arm and low power loss, which results in a compact and efficient 90° three-branch beam splitter.

Fig. 3 shows the proposed 90° beam splitter. This structure can be obtained from the simple waveguide junction of Fig. 1
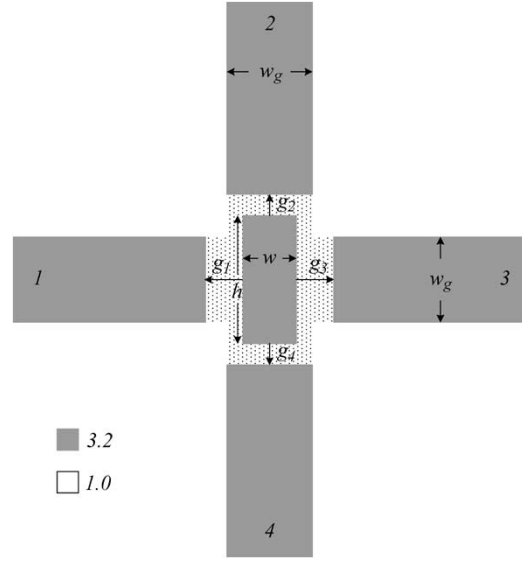
by replacing the lightly shaded area with air, thus, forming a rectangular cavity. The width w of the rectangular cavity is chosen to be smaller than the waveguide width w_g in order to ensure coupling to the resonant cavity mode with an even symmetry in the horizontal direction. The height h is chosen to be larger than the waveguide core width. The axes of the rectangular cavity are chosen to always coincide with the axes of the horizontal and vertical waveguides. The widths of the air gaps g_1, g_2, g_3, and g_4 are generally different in value. The widths of the air gaps in the horizontal direction (g_1, g_3) are always taken to be $\geq (w_g - w)/2$. The four air gaps are used to control the power splitting ratio among the output arms of the beam splitter and to tune the device operation. For instance, in order to have higher power coupling in the forward output arm, the width of the air gap g_3 is reduced. Numerical simulations done in order to demonstrate the operation of the proposed device will be presented in the next section. The cavity parameters and the air gaps were selected through a number of repeated simulations using the MOL, while monitoring the device response, with an emphasis on the modal reflectivity and the FPR in order to ensure that they remain sufficiently low.

III. NUMERICAL RESULTS

When the air gaps g_2 and g_4 associated with the vertical arms are equal in value (symmetric beam splitter), the optical powers coupled to those arms are also equal. However, when $g_2 \neq g_4$ (asymmetric beam splitter), the powers in the vertical arms are no longer expected to be the same. Both of these cases will be addressed. Throughout this work, the waveguide core width and the refractive index were fixed at $w_g = 0.2$ μm and $n = 3.2$, respectively.

Fig. 4(a)–(c) shows the calculated spectral response of the proposed beam splitter using the following parameters: $w = 60$ nm; $h = 620$ nm; $g_1 = 110$ nm; $g_2 = g_4 = 120$ nm; and $g_3 = 140$ nm. The modal reflectivity R_1, which is shown in Fig. 4(a), is generally low in value over the entire wavelength
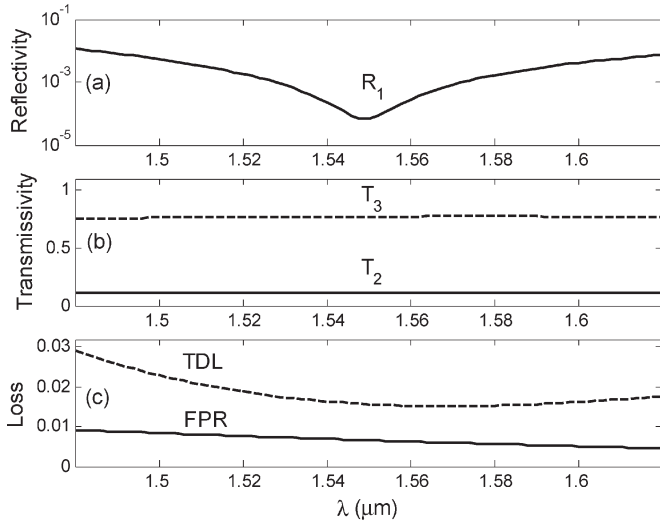
Fig. 4. Spectral response of the symmetric beam splitter corresponding to low power transmission in the vertical arms.
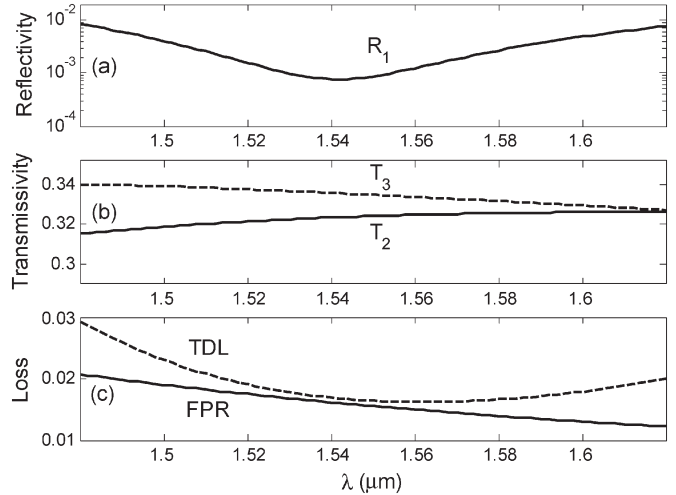
Fig. 6. Spectral response of the symmetric beam splitter showing nearly equal power transmission in all the output arms.
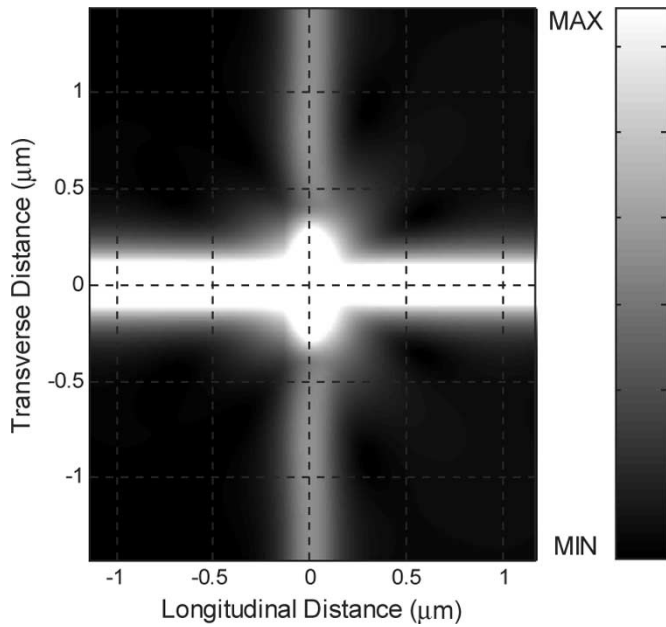
Fig. 5. Electric field intensity image in the symmetric beam splitter (at $\lambda = 1.55\ \mu m$) corresponding to low power transmission in the vertical arms.
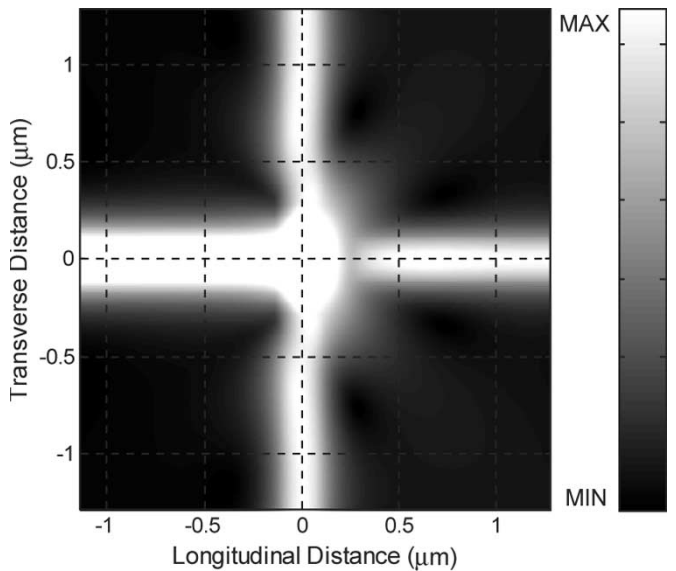
Fig. 7. Electric field intensity image in the symmetric beam splitter (at $\lambda = 1.55\ \mu m$) with nearly equal power transmission in the output arms.

range with a minimum value of approximately 6.8×10^{-5} at $\lambda = 1.55\ \mu m$. The transmissivities ($T_2 = T_4$, and T_3) shown in Fig. 4(b) all have flat responses. For this reason, the spectral width $\Delta\lambda$ will be based on the modal reflectivity curve only, using the arbitrary measure of $R_1 \leq 5 \times 10^{-3}$ to define it. Based on this measure, $\Delta\lambda \approx 100$ nm in this particular case. Fig. 4(b) shows that most of the optical power is coupled to the forward arm ($T_2 \approx 0.77$) of the device and some of the power is coupled to the upper and the lower vertical arms ($T_2 = T_4 \approx 0.11$) of the structure. The variations of the FPR and the TDL with wavelength are shown in Fig. 4(c), which indicates that both are generally low in value (FPR < 0.01, TDL < 0.03). The electric field intensity image around the junction at $\lambda = 1.55\ \mu m$ (see Fig. 5) shows that most of the optical power is coupled to the forward arm of the device. The absence

of a standing wave pattern in the input arm indicates that the amount of power reflected is very low in this case.

When the air gap g_3 associated with the forward arm is increased (while keeping the remaining parameters fixed), the power coupled to the forward arm is reduced in value. By doing so, the device operation is, however, degraded, resulting in increased reflectivity and increased FPR. This necessitates tuning of the remaining five parameters of the device so that low reflectivity and low FPR are maintained. The following set of parameters, i.e., $w = 60$ nm, $h = 530$ nm, $g_1 = 110$ nm, $g_2 = g_4 = 30$ nm, and $g_3 = 250$ nm, represents a tuned set of parameters when g_3 is increased from $g_3 = 140$ nm, associated with the previous case, to $g_3 = 250$ nm. Fig. 6(a)–(c) shows the spectral response of the beam splitter when the new set of parameters is used. Again, the reflectivity curve [see Fig. 6(a)] is low with a value of about 8.66×10^{-4} at $\lambda = 1.55\ \mu m$ and $\Delta\lambda \approx 100$ nm. The modal transmissivity in the forward arm T_3 shown in Fig. 6(b) has decreased in value, while the modal
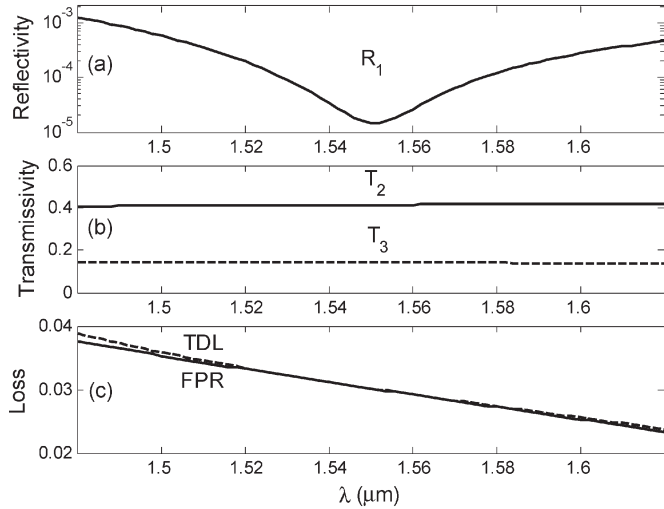
Fig. 8. Spectral response of the symmetric beam splitter corresponding to maximum power transmission in the vertical arms.
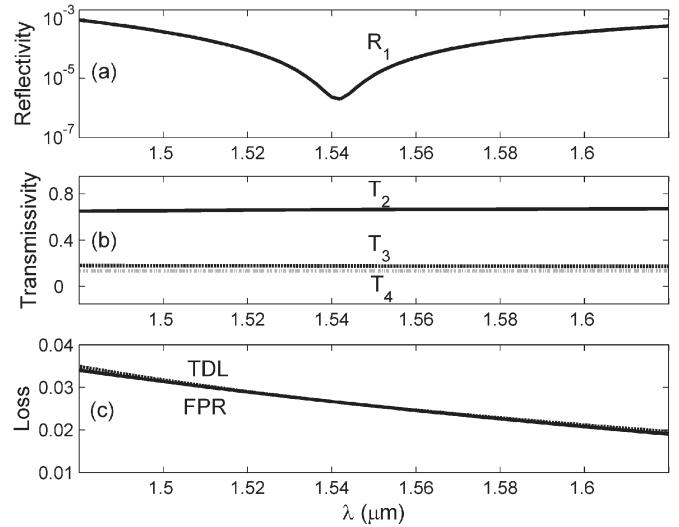
Fig. 10. Spectral response of the asymmetric beam splitter corresponding to maximum power transmission in the upper vertical arm.
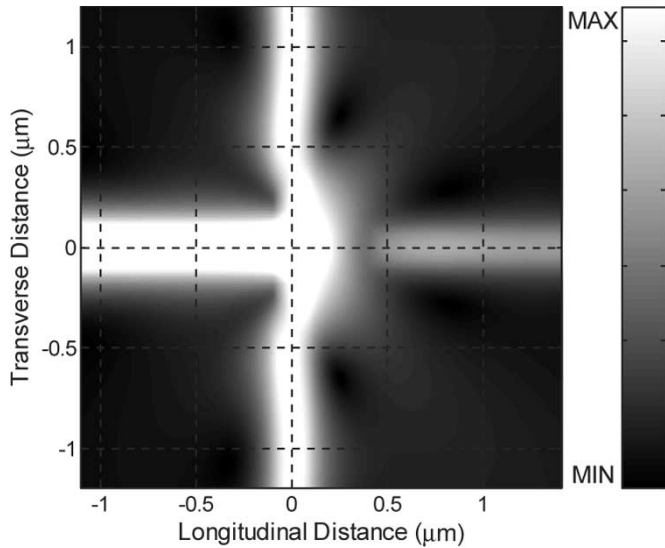
Fig. 9. Electric field intensity image in the symmetric beam splitter (at $\lambda = 1.55$ μm) corresponding to maximum power transmission in the vertical arms.
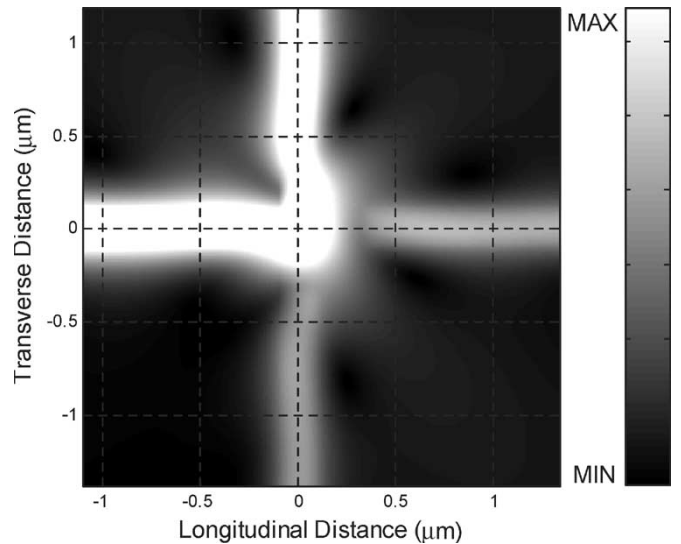
Fig. 11. Electric field intensity image in the asymmetric beam splitter (at $\lambda = 1.55$ μm) corresponding to maximum power transmission in the upper vertical arm.

transmissivity in the vertical arms $(T_2 = T_4)$ has increased. In this particular case, the transmissivity in the three output arms are approximately equal in value $(T_2 = T_4 \approx T_3 \approx 0.32)$. As seen in Fig. 6(c), the FPR has increased in this case with a maximum value of about 0.02. The TDL at $\lambda = 1.55$ μm equals approximately 0.016. At the lowest and the highest wavelengths shown in Fig. 6(c), the values of the TDL are approximately 0.029 and 0.020, respectively. Fig. 7 shows nearly equal field intensity in all the output arms at $\lambda = 1.55$ μm. This case is of special interest because of the nearly equal power splitting ratio in the output arms of the proposed device. For this reason, later in this section, two possible approaches are presented in order to further reduce the TDL in this special case.

When the air gap in the forward arm is increased beyond its current value of $g_3 = 250$ nm, the power in the forward arm is expected to decrease further. In order to examine this possibility, the spectral responses were calculated using the following set of tuned parameters: $w = 80$ nm;

$h = 230$ nm; $g_1 = 60$ nm; $g_2 = g_4 = 80$ nm; and $g_3 = 370$ nm. Fig. 8(a)–(c) shows the resulting spectral responses. In particular, Fig. 8(b) shows that $T_2 = T_4$ has substantially increased to about 0.41, while T_3 has decreased to about 0.14. The value $T_2 = T_4 \approx 0.41$, is the maximum transmissivity we were able to obtain for the symmetric beam splitter. The spectral width corresponding to this case exceeds the horizontal range of Fig. 8. The FPR and the TDL also increase in this case. However, they remains acceptably low, having values less than 0.04. The field intensity image at $\lambda = 1.55$ μm, corresponding to this case, is shown in Fig. 9.

In all of the above cases, the beam splitter has been assumed to be symmetric with respect to the horizontal by choosing the air gap widths g_2 and g_4 to be equal. When one of these air gaps is increased in value with respect to other, for instance, when $g_4 > g_2$, the power coupled to the upper vertical arm should increase with respect to the power coupled to the lower

TABLE I
SUMMARY OF TUNED PARAMETER VALUES USED IN THE VARIOUS REPORTED CASES. THE VALUES OF $R_1, T_2, T_3, T_4, \Delta\lambda$,
AND THE FPR CORRESPOND TO $\lambda = 1.55\ \mu$m. THE SECOND ROW OF THE TABLE CONTAINS THE TUNED PARAMETERS
FOR MAXIMUM POWER TRANSMISSION IN THE FORWARD ARM

w(nm)	h(nm)	g_1(nm)	g_2(nm)	g_3(nm)	g_4(nm)	R_1	T_2	T_3	T_4	FPR	$\Delta\lambda$ (nm)
90	350	55	500	55	500	8.56(-5)	5.62(-3)	9.84(-1)	5.62(-3)	4.34(-3)	140
60	620	110	120	140	120	6.78(-5)	1.11(-1)	7.71(-1)	1.11(-1)	6.57(-3)	100
60	530	110	30	250	30	8.66(-4)	3.24(-1)	3.34(-1)	3.24(-1)	1.55(-2)	100
80	230	60	80	370	80	1.48(-5)	4.14(-1)	1.41(-1)	4.14(-1)	3.02(-2)	140
80	220	60	20	300	220	1.29(-5)	6.63(-1)	1.76(-1)	1.34(-1)	2.56(-2)	140
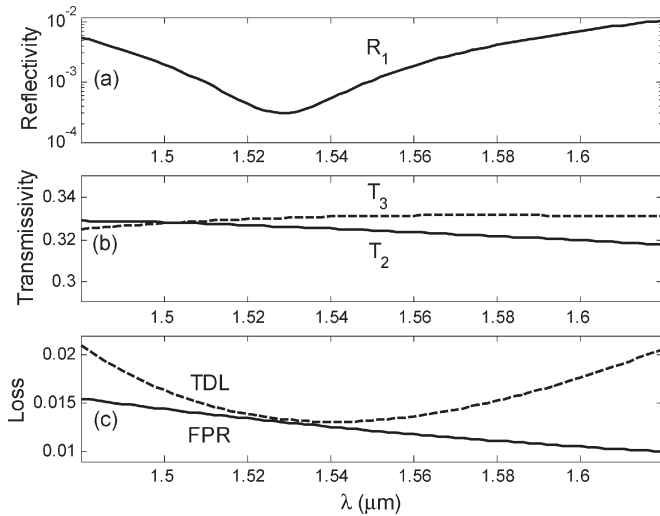
Fig. 12. Spectral response of the symmetric beam splitter with a horizontally shifted rectangular cavity, showing nearly equal power transmission in all the output arms.

Fig. 13. Three-branch 90° beam splitter with a horizontally shifted rectangular resonant cavity and four identical metal strips.

vertical arm. We have tested this assumption by using the following set of tuned parameters: $w = 80$ nm; $h = 220$ nm; $g_1 = 60$ nm; $g_2 = 20$ nm; $g_3 = 300$ nm; and $g_4 = 220$ nm. The air gap $g_2 = 20$ nm is chosen to be much smaller than $g_4 = 220$ nm in order to maximize power coupling in the upper vertical arm while maintaining low modal reflectivity. The modal reflectivity corresponding to this case, which is shown in Fig. 10(a), is very low. As expected, T_2 attains a large value of $T_2 \approx 0.66$ as compared to $T_3 \approx 0.17$ and $T_4 \approx 0.13$, as seen in Fig. 10(b). The FPR and the TDL curves for this case are shown in Fig. 10(c), which remains below 0.04. The field intensity image at $\lambda = 1.55\ \mu$m, corresponding to this case is shown in Fig. 11, where it is clearly seen that most of the optical power is channeled into the upper vertical arm.

The above results are summarized in Table I. The reported values of R_1, T_2, T_3, T_4, and FPR correspond to $\lambda = 1.55\ \mu$m. The second row of Table I contains additional data that corresponds to the special case when the beam splitter couples maximum power in the forward arm giving $T_3 \approx 0.98$ and very low power in the remaining arms ($T_2 = T_4 \approx 0.006$). In all the cases, the spectral width exceeds 100 nm while the FPR and the TDL remain below 0.04.

In the special case of nearly equal power splitting discussed above, the TDL at $\lambda = 1.55\ \mu$m equals 0.0163 (0.071 dB). This value of the TDL can be further reduced. Two possible

approaches for reducing the TDL are presented next. First, there is another degree of freedom that can be used to improve the device performance. This corresponds to shifting (in the horizontal direction) the vertical axis of the rectangular cavity with respect to the axis of the vertical arms. Second, the radiative part of the field can be suppressed by the use of metallic strips suitably placed at the four corners of the beam splitter, which helps in reducing the TDL. Both of these proposed methods can be used simultaneously in order to have an accumulative reduction of the TDL, as will be demonstrated later.

Using the same set of parameters corresponding to the nearly equal power splitting discussed earlier, the rectangular cavity is shifted to the left by 15 nm in such a way that the horizontal air gaps (g_1 and g_3) remain unchanged. The resulting device response corresponding to this case is shown in Fig. 12(a)–(c). The nearly equal power splitting is maintained in this case as seen in Fig. 12(b). In addition, the TDL at $\lambda = 1.55\ \mu$m
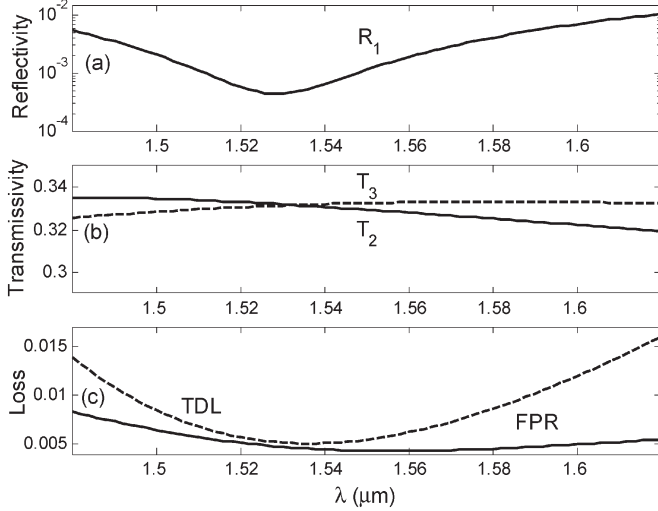
Fig. 14. Spectral response of the symmetric beam splitter with a horizontally shifted rectangular cavity and four identical metal strips, showing nearly equal power transmission in all the output arms and reduced total device loss.

equals 0.0132 (0.057 dB) in this particular case, which is less than the previously reported value of 0.0163 (0.071 dB), which corresponds to no shift of the rectangular cavity.

Fig. 13 shows the beam splitter with the horizontally shifted rectangular cavity. In addition, it also shows four identical rectangular strips made of silver, placed at the four corners of the device. The dimensions and exact location of these strips are indicated in the figure, which were selected to minimize the TDL. The four metallic strips are symmetrically placed with respect to the horizontal and vertical waveguide ends. The refractive index of silver is taken as $n_{silver} = 0.514 + j10.8$ at $\lambda = 1.55$ μm. It is known that the complex refractive index of silver is highly wavelength dependent. However, in the numerical simulation to be presented later, the refractive index of silver is assumed to be independent of wavelength and is fixed at the above-indicated value. This is done because it has been observed that accounting for the wavelength dependence of the refractive index of silver had a negligible effect on the calculated results.

The device response corresponding to this new case is shown in Fig. 14(a)–(c). It is clearly seen that the addition of the metallic strips results in a further reduction of the TDL. The TDL decreases to 0.0054 (0.023 dB) at $\lambda = 1.55$ μm, which is substantially less than the previously reported value of 0.0132 (0.057 dB), corresponding to the horizontally shifted rectangular cavity [see Fig. 12(c)].

IV. CONCLUSION

A three-branch 90° beam splitter that utilizes a rectangular resonant cavity at the center has been numerically demonstrated. By adjusting the air gap widths and the dimensions of the rectangular cavity, various power splitting ratios can be obtained while maintaining low modal reflectivity and low fraction of the power radiated (FPR) over a reasonably wide range of wavelength. For the symmetric beam splitter, the power in the vertical arms can be varied from extremely low values to a maximum value of about 0.41. In addition, it is

possible to have nearly equal power transmission in all the output arms of the beam splitter. In the case of the asymmetric beam splitter, the power coupled to one of the vertical arms can reach as high as 0.66. In the case of equal power splitting, by slightly shifting the rectangular cavity in the horizontal direction and simultaneously adding identical metallic strips at the four corners of the device, the TDL at $\lambda = 1.55$ μm is reduced by approximately a factor of 3, resulting in a TDL of about 0.023 dB. Because it is possible to design the proposed beam splitter to have a negligibly small modal reflectivity, two or more of these devices, which may have the same or different power splitting ratios, can be cascaded in the horizontal and the vertical directions, giving rise to a more complex beam splitting system.

APPENDIX
BASIC MOL FORMULATION

A brief outline of the basic MOL formulation is presented in this Appendix. The reader is referred to the cited references [13]–[17], which contain important and useful extensions of this method.

The two-dimensional time harmonic wave equation is given by

$$\frac{\partial^2 \psi}{\partial x^2} + \frac{\partial^2 \psi}{\partial z^2} + k_0^2 n^2 \psi = 0 \tag{A1}$$

where $\psi = \psi(x, z)$ represents the electric field E_y of TE polarized waves. $k_0 = 2\pi/\lambda$ is the free space wave number, and $n = n(x)$ is the refractive index of the medium. Upon discretization of $\partial^2 \psi / \partial x^2$ into N sample points of mesh size Δx, using the central difference approximation, (A1) can be written in the following matrix form:

$$\frac{d^2 \overline{\Psi}(z)}{dz^2} + \overline{Q}^2 \overline{\Psi}(z) = 0 \tag{A2}$$

where the column vector $\overline{\Psi} = [\psi_1 \ \psi_2 \ \cdots \ \psi_N]^t$ contains the discretized values of the field, and the square matrix $\overline{Q}^2$ is given by

$$\overline{Q}^2 = \frac{1}{\Delta x^2} \begin{bmatrix} -2 & 1 & 0 & . & . & . \\ 1 & -2 & 1 & 0 & . & . \\ 0 & 1 & -2 & 1 & 0 & . \\ . & . & . & . & . & . \\ . & . & 0 & 1 & -2 & 1 \\ . & . & . & 0 & 1 & -2 \end{bmatrix}$$

$$+ k_0^2 \begin{bmatrix} n_1^2 & 0 & . & . & . & . \\ 0 & n_2^2 & 0 & . & . & . \\ . & 0 & n_3^2 & 0 & . & . \\ . & . & . & . & . & . \\ . & . & . & 0 & n_{N-1}^2 & 0 \\ . & . & . & . & 0 & n_N^2 \end{bmatrix} \tag{A3}$$

where the tridiagonal and the diagonal matrices represent the discretized values of $\partial^2 \psi / \partial x^2$ and $n^2(x)$, respectively.

The general solution of the above ordinary matrix differential (A2) is given by

$$\overline{\Psi} = e^{j\overline{Q}z}A + e^{-j\overline{Q}z}B \qquad (A4)$$

where $e^{\pm j\overline{Q}z}$ account for the forward and backward fields, respectively. The exponential terms $e^{\pm j\overline{Q}z}$ are calculated by first computing the eigenvalue matrix $\overline{\Lambda}^2$ and the eigenvector matrix $\overline{T}$ of the square matrix $\overline{Q}^2$, so that $\overline{Q}^2 = \overline{T}\,\overline{\Lambda}^2\overline{T}^{-1}$ and, thus, $e^{\pm j\overline{Q}z} = \overline{T}e^{\pm j\overline{\Lambda}z}\overline{T}^{-1}$.

REFERENCES

[1] H. B. Lin, R. S. Cheng, and W. S. Wang, "Wide-angle low loss single mode symmetric Y-junctions," *IEEE Photon. Technol. Lett.*, vol. 6, no. 7, pp. 825–827, Jul. 1994.

[2] W. C. Chang and H. B. Lin, "A novel low-loss wide-angle Y-branch with a diamond-like microprism," *IEEE Photon. Technol. Lett.*, vol. 11, no. 6, pp. 683–685, Jun. 1999.

[3] C. W. Hsu, H. L. Chen, and W. S. Wang, "Compact Y-branch power splitter based on simplified coherent coupling," *IEEE Photon. Technol. Lett.*, vol. 15, no. 8, pp. 1103–1105, Aug. 2003.

[4] K. Shirafuji and S. Kurazono, "Transmission characteristics of optical asymmetric Y-junction with a gap region," *J. Lightw. Technol.*, vol. 9, no. 4, pp. 426–429, Apr. 1991.

[5] H. B. Lin, J. Y. Su, R. S. Cheng, and W. S. Wang, "Novel optical single-mode asymmetric Y-branches for variable power splitting," *J. Quantum Electron.*, vol. 35, no. 7, pp. 1092–1096, Jul. 1999.

[6] H. B. Lin, Y. H. Wang, and W. S. Wang, "Single mode 1×3 integrated optical branching circuit design using microprism," *Electron. Lett.*, vol. 30, no. 5, pp. 408–409, Mar. 1994.

[7] T. J. Wang, Y. H. Wang, and W. S. Wang, "Single mode 1×3 equal power divider using a substrate microprism and two waveguide expanders," *IEEE Photon. Technol. Lett.*, vol. 12, no. 2, pp. 164–166, Feb. 2000.

[8] W. Y. Hung, H. P. Chan, and P. S. Chung, "Single-mode 1×3 integrated optical branching circuit design using phase-front accelerators," *Electron. Lett.*, vol. 24, no. 22, pp. 1365–1366, Oct. 1988.

[9] S. Banba and H. Ogawa, "Novel symmetrical three-branch optical waveguide with equal power division," *IEEE Microw. Guided Wave Lett.*, vol. 2, no. 5, pp. 188–190, May 1992.

[10] T. Yabu, M. Geshiro, N. Minami, and S. Sawa, "Symmetric three-branch optical power divider with a coupling gap," *J. Lightw. Technol.*, vol. 17, no. 9, pp. 1693–1699, Sep. 1999.

[11] T. J. Wang, C. F. Huang, and W. S. Wang, "Wide-angle 1×3 optical power divider in LiNbO$_3$ for variable power splitting," *IEEE Photon. Technol. Lett.*, vol. 15, no. 10, pp. 1401–1403, Oct. 2003.

[12] H. C. Song, T. W. Oh, S. Y. Shin, S. Y Yi, W. H. Jang, and T. H. Rhee, "Four branch single-mode waveguide power divider," *IEEE Photon. Technol. Lett.*, vol. 10, no. 12, pp. 1760–1762, Dec. 1998.

[13] R. Pregla and E. Ahlers, "The method of lines for the analysis of discontinuities in optical waveguides," *Electron. Lett.*, vol. 29, no. 21, pp. 1845–1847, Oct. 1993.

[14] W. D. Yang and R. Pregla, "Method of lines for analysis of waveguide structures with multidiscontinuities," *Electron. Lett.*, vol. 31, no. 11, pp. 892–893, May 1995.

[15] H. A. Jamid and M. N. Akram, "A new higher order finite-difference approximation scheme for the method of lines," *J. Lightw. Technol.*, vol. 19, no. 3, pp. 398–404, Mar. 2001.

[16] ——, "Analysis of deep waveguide gratings: An efficient cascading and doubling algorithm in the method of lines framework," *J. Lightw. Technol.*, vol. 20, no. 7, pp. 1204–1209, Jul. 2002.

[17] A. A. Shittu, S. Al-Bader, and H. Jamid, "Mode reflectivity of finitely-periodic dielectric waveguides," *Opt. Commun.*, vol. 114, no. 3–4, pp. 242–246, Feb. 1995.

[18] C. Manolatou, S. G. Johnson, S. Fan, P. R. Villeneuve, H. A. Haus, and J. D. Joannopoulos, "High-density integrated optics," *J. Lightw. Technol.*, vol. 17, no. 9, pp. 1682–1692, Sep. 1999.

[19] S. G. Johnson, C. Manolatou, S. Fan, R. Villeneuve, J. D. Joannopoulos, and H. A. Haus, "Elimination of crosstalk in waveguide intersections," *Opt. Lett.*, vol. 23, no. 23, pp. 1855–1857, Dec. 1998.

H. A. Jamid, photograph and biography not available at the time of publication.

M. Z. M. Khan, photograph and biography not available at the time of publication.

M. Ameeruddin, photograph and biography not available at the time of publication.